AUTOMATIC STEERING CONTROL IN TRACTOR SEMI-TRAILER VEHICLES FOR LOW SPEED MANEUVERABILITY ENHANCEMENT

Journal:	*Proceedings of the Institution of Mechanical Engineers, Part K: Journal of Multibody Dynamics*
Manuscript ID	JMBD-16-0012.R2
Manuscript Type:	Original Article
Date Submitted by the Author:	27-Apr-2016
Complete List of Authors:	Abroshan, Mehdi; Iran University of Science and Technology, Automotive Engineering Taiebat, Morteza; University of British Columbia Goodarzi, Avesta; University of Waterloo, Mechanical and Mechatronics Khajepour, Amir; University of Waterloo, Mechanical and Mechatronics
Keywords:	Active safety system, Maneuverability, Tractor semi-trailer, All-Wheel Steering, Steering Control
Abstract:	In this paper, a controller for an automated steering articulated vehicle with the special capability to reduce off tracking in low speed manoeuvres is proposed. Conventional tractor-trailers have a large off tracking in low-speed manoeuvres. In the proposed vehicle, all wheels of the tractor and trailer are steerable (All Wheel Steering- AWS). The controllers of the tractor and trailer work independently, and each one consists of two layers. A fuzzy controller and a PID controller are designed in the upper and lower layer, respectively, to control the actuators. The aim of the controller is to ensure that the end points of both the tractor and the trailer exactly follow the path of tractor's first point. To assess the performance of proposed controller as well as steerability effect of all wheels in low speeds, the TruckSim simulation software is used. The simulation results confirm that the proposed approach improves the manoeuvrability and accuracy of path tracking not only compared to conventional vehicles, but also to the

	Conventional Tractor – Active Trailer (CT-AT) scheme, which was previously proposed by a number of studies. Additionally, it reduces lateral tyre forces to enhance the working life.

AUTOMATIC STEERING CONTROL IN TRACTOR SEMI-TRAILER VEHICLES FOR LOW SPEED MANEOUVRABILITY ENHANCEMENT

M. Abroshan[1)], M. Taiebat[2)], A. Goodarzi[3)*1] And A. Khajepour[3)]

[1)]Department of Automotive Engineering, Iran University of Science & Technology, Narmak, Tehran, Iran
[2)]Department of Mechanical Engineering, University of British Columbia, Vancouver, BC, V6T 1Z4, Canada
[3)]Mechanical and Mechatronics Engineering Department, University of Waterloo, Waterloo, ON, N2L 3G1, Canada

ABSTRACT

In this paper, a controller for an automated steering articulated vehicle with the special capability to reduce off tracking in low speed manoeuvres is proposed. Conventional tractor-trailers have a large off tracking in low-speed manoeuvres. In the proposed vehicle, all wheels of the tractor and trailer are steerable (All Wheel Steering- AWS). The controllers of the tractor and trailer work independently, and each one consists of two layers. A fuzzy controller and a PID controller are designed in the upper and lower layer, respectively, to control the actuators. The aim of the controller is to ensure that the end points of both the tractor and the trailer exactly follow the path of tractor's first point. To assess the performance of proposed controller as well as steerability effect of all wheels in low speeds, the TruckSim simulation software is used. The simulation results confirm that the proposed approach improves the manoeuvrability and accuracy of path tracking not only compared to conventional vehicles, but also to the Conventional Tractor – Active Trailer (CT-AT) scheme, which was previously proposed by a number of studies. Additionally, it reduces lateral tyre forces to enhance the working life.

KEYWORDS: Active safety system, Off-tracking, Manoeuvrability, Tractor semi-trailer, All-Wheel Steering

1. INTRODUCTION

In recent years, a great amount of work has been undertaken on vehicle automation. The purpose of these studies is to enhance the transportation performance and safety [1-4]. Since commercial vehicles have a large share in transportation and transit systems, a number of vehicle manufacturers have recently introduced their self-steering articulated vehicles. This is an important step toward the fully autonomous versions. It is obvious that such vehicles should be manoeuvrable in limited spaces and be accurate in tracking the path. Hence, the investigations regarding the performance enhancement of this class of vehicles are important current topics in literature.

* Corresponding author: e-mail: avesta.goodarzi@uwaterloo.ca

Large vehicles such as articulated tractor-trailers and semi-trailers suffer from limited manoeuvrability and path tracking [5, 6] The large distance between the tractor axels as well as the length of trailer creates several issues. First, these large lengths cause a large turning radius that makes the vehicle unmanoeuvrable in tight spaces. Also, the rear end of the tractor and trailer does not follow the path passed by the front end of the tractor. This phenomenon is called *'off-tracking'*. Off tracking significantly reduces the vehicle path following accuracy [7] These shortages make articulated vehicles less attractive choices for urban freight sector, specially where the urban structures such as intersections and roundabouts oblige a highly limited space for turning [8, 9].

For a tractor as a single-unit-truck with long wheelbase, the steerability of the rear wheels can reduce the turning radius and increase manoeuvrability. In order to decrease the turning radius in a curve, the rear wheels should be steered in the opposite direction to the front wheels. To steer the rear wheels of a conventional vehicle a hydraulic system can be employed [10]. Whereas, in electric vehicles, it is possible to use two electric motors for each wheel individually in order to provide independent traction and steering angle [11] In these vehicles that all wheels are steerable, using an appropriate steering strategy is essential.

For a semi-trailer, it usually consists of several axles that normally are not steerable. In sharp manoeuvres, the unsteerable characteristic of trailer causes large off tracking and also creates large lateral forces in the tyres. This exacerbates tyre wear and also damages the road surface [12]. Hence, in order to make the trailer steerable, several active and passive steering algorithms have been proposed. Their low cost and simple structure of passive systems caused them to be widely used in conventional designs [13]. They use simple strategy such as 'a fixed rear-to-front wheel steer angle ratio 'and can reduce the turning radius and the off tracking increases simultaneously [10].

Although these systems increase manoeuvrability and reduce lateral forces at low speeds, they have two unattractive consequences: amplification of tail rotation in transient conditions and reduction of vehicle stability at high speeds. In order to maintain vehicle stability, some passive systems have a strategy to lock the system at high speeds. It should be noted that by increasing trailer steerability, tail rotation would also increase [12, 14-16]. Because of the shortcomings of passive systems, active control systems have been studied in different researches. These pieces of research take advantage of active control of trailer's wheels steering angles by different strategies in order to control stability, roll over, and increasing manoeuvrability. Their outcomes exhibit that active control of a trailer-wheels' steering has a major role in vehicle safety and stability [17-22]. In 2011, Md. Manjurul Islam et al. [17] developed a kinematic method to design articulated vehicles with steerable trailer wheels. In this method, design parameters are optimized for trade offs between increasing manoeuvrability and path tracking performance in low speeds and enhancing stability in high speeds. The controller is a Linear Quadratic Regulator (LQR), which has two distinct control modes for high and low speeds. However, this controller is not able to optimize the vehicle's operation in a wide range of speeds.

Odhams et al. developed an active control steering strategy for trailers based on the methodology of Notsun [23]. This was to be used both at low and high speeds. In this strategy, titled Conventional Tractor – Active Trailer (CT-AT), the trailer is navigated in a way that the rear end of it follows the fifth wheel's path. The goal of this controller is to follow the desired path by minimizing tyre lateral forces and the determining the axle's steer angle, accordingly. In that study, the trailer's axles' steering angles are determined based on a kinematic model of the trailer and the difference between angle of the trailer's rear end and target path, all of which is regulated with a PID controller. However, at high speeds, the steering angle is determined using the PID controller based on dynamic model of a pendulum. The performance of this vehicle is assessed with a Roundabout test for low speeds and a Lane Change test for high speeds. Although the results show improvement in reduction of off tacking and tyre's lateral forces in both high and low speeds, due to the large wheelbase of tractor and passing the rear end of trailer from fifth wheel's path, the offset from target path is still large. In assessing the performance of their controller, the results from the Roundabout test have shown that lateral forces are drastically reduced. Additionally, tail rotation is entirely eliminated. It also confirmed that the controller was able to considerably moderate the maximum off tracking from target path. These studies claim that the unsteerability of the rear wheels of the tractor leads to this residual off tracking in articulated vehicles, and by removing this constraint; it is possible to further decrease off tracking [24, 25]. Oreh et al. in 2012, proposed a new desired articulation angle for articulated vehicles ensuring the rear end of the trailer tracks the path passed by fifth wheel. In this method, position of rear end point of trailer is predicted by kinematic equations and Taylor's series then according to the deviation, the proper articulation angle is calculated [26].

Inspired by rotating vehicles with independently controllable steering and traction of each wheel [27-29] in this study, the independent steerability along with wide steering range for all wheels of tractor and trailer is considered, in order to increase manoeuvrability of the vehicle and minimize off tracking. Moreover the traction of the rear wheels can be controlled independently. Two independent controllers in two layers control the steering angle of the tractor and trailer as well as the traction of the tractor. Hence, the tractor and trailer have minimum off tracking in navigation through sharp manoeuvres.

In looking at controller design, since path following and vehicle dynamic control are sophisticated issues, classic controllers are not providing enough accuracy [1]. These types of controllers require an explicit linear mathematical model, but this problem has a nonlinear nature [2, 30, 31]. A fuzzy controller without a precise mathematical model can use human experience/knowledge, which makes the system have human-like behavior. Therefore, in order to determine the instant centre of rotation in the tractor, a fuzzy controller is used in the upper layer of the tractor control system. A similar controller is also used to regulate the optimal yaw rate in a semi-trailer. In the lower layer, a simple and well-known PID controller is used to adjust angular speed in each wheel. The details of the method are described thoroughly in following sections.

2. CONCEPT AND METHODOLOGY

In previous studies, the concept of control points is shown as an effective approach to study path tracking problem for passenger cars [32, 33] Considering the importance of off tracking in commercial articulated vehicles, this method can be extended for those as well. As shown in Figure 1, three points are considered on the tractor semi-trailer. These three points are named (A) Tractor Front End Point, (B) Tractor Rear End Point and (C) Trailer Rear End Point. In this method, instead of the common method, which uses the lateral offset of vehicle's centre of gravity and its heading angle compared to the target path, the lateral offsets of control points on longitudinal axis of vehicle are considered as the state variables of the control system [32, 34, 35].

Figure 1. Parameter definition for the vehicle.

During the manoeuvre, these three points have lateral offsets with respect to the target path. Therefore, the ultimate goal of the controller is to compensate for them. Placing the point (A) on the target path is similar to the driver's behavior in conventional vehicles, which tries to maintain the vehicle nose on the path. Furthermore, placing (B) and (C) on the path indicates removing off tracking in the tractor and trailer.

Commonly, the tractor's wheels steer based on Ackerman steering geometry. This geometry itself is based on free-rolling of all wheels. As shown in Figure 1, all wheels must turn around a common point, which is named *Instant Centre of Rotation (ICR)*. This geometry is efficiently practical at low speeds [11, 28, 36, 37].

Obviously, by changing the ICR position in longitudinal and lateral directions, the turning radius of points A and B can be changed. This way, they will be placed on the target path with minimum lateral offset. Consequently, the goal of the upper layer controller of the tractor is to determine the tractor's ICR with two components x_{ICR} and y_{ICR} in relation to the geometric centre of tractor.

In controller design, placing the first point on the target path is a higher priority than the second point. According to Figure 1, turning radius of point (A) can be calculated by equation (1). Since longitudinal coordinate and lateral coordinate of ICR vary in range of [-1.85 1.85] which is the track of the tractor and [-∞ +∞] (theoretically) respectively, it is clear that ${y_{ICR}}^2 \gg (x_A - x_{ICR})^2$ which means changing y_{ICR} is more effective in turning radius than the other component. In addition, changing direction of rotation is only possible by changing direction of y_{ICR}. Therefore, y_{ICR} is used to reduce the offset of point (A) while x_{ICR} is used to reduce the offset of point B. For example, as shown in figure (1), the current position of the tractor's ICR has resulted in an increase in the offset of point A. Thus, to reduce it, the lateral coordinate of ICR must be transferred to the positive side of y-axis.

$$R_A = \sqrt{(x_A - x_{ICR})^2 + {y_{ICR}}^2} \tag{1}$$

The only degree of freedom between the tractor and the trailer is the hinged movement around the fifth wheel. Hence, to reduce trailer rear end point offset, yaw rate should be controlled by applying the appropriate steering angle. As shown in Figure 1, by adding the appropriate yaw rate r_{ST} in the kinematic equation, the rear end of the trailer can be navigated to the target path. The trailer steering angles are defined via ICR of trailer, which is separate from the tractor's.

In this study, determining the lateral offset of three points is the first step in controller design. The first point's offset from the target path is measured through sensors. Whereas, to determine rear end point of trailer and tractor offset, the coordinates of the target path are calculated from kinematic estimators, and then, B and C's offsets from the target path are determined from comparing current values and desired values. These estimators and the procedure of off tracking derivation have been expanded upon in the Appendix A.

The assumption of using sensors data for the first point is valid and practical with the development of image processing technology and visual systems. Many studies has been carried out on path recognition and determining the required information from an image. This system, which is widely developing in automated and semi-automated vehicles, is used to instantly extract information such as lateral and angular offsets of vehicle compared to its target path [1, 30, 38, 39].

Now by having the lateral offset of these three, the controller design can be incorporated.

3. CONTROLLER DESIGN

Figure 2 illustrates the system's block diagram for the controller design. This hierarchical controller consists of upper and lower layers. In the lower layer, a PID controller is used to adjust the required torque for each wheel. Using the angular speed error of each wheel, the PID determines the optimal voltage across the electric motor. A fuzzy controller in the upper layer is designed independently for the trailer and the tractor with two different strategies

Figure 2. Block diagram of the proposed controller.

In the tractor's upper layer, a fuzzy controller reduces offsets of points A and B by determining the ICR in each instant. The trailer's fuzzy controller reduces offset of point C by determining instant proper yaw rate. In all designed fuzzy controllers, Mamdani reasoning method and Centroid method in De-fuzzification are used. Furthermore, triangular and trapezoidal functions are used as the membership functions. These simple linear membership functions reduce the computational burden, which are easy to tune. The linguistic terms of the membership functions are presented in Table 1.

Table 1. Lingustic terms definition.

3.1. Tractor's upper layer controller

The ICR is composed of two components longitudinal (x_{ICR}) and lateral (y_{ICR}) coordinates in relation to the geometric centre. Changing y_{ICR} in one side causes a change in turning radius of points (A) and (B). A shift from positive side to negative side or vice versa causes a change in steering angle direction. Additionally, a change in x_{ICR} changes the turning radius of the first and end points in relation to each other. It is the same as determining a varying coefficient for the rear wheel steering angle in relation to the front wheel steering angle. It should be noted that the determination of x_{ICR} and y_{ICR} in one fuzzy controller increases the number of fuzzy rules that substantially increases computing time. That is the reason for using the hierarchical method.[40]

When tractor moves in a straight line, y_{ICR} approaches infinity to show zero steering angle. During the manoeuvre, depending on the severity, y_{ICR} must get close to the vehicle, Hence y_{ICR} has to move in a wide range. In addition, according to Figure 1 (in the context) and the equation (2), y_{ICR} and the steering angle have a tangent relationship. Therefore, it is hard to consider y_{ICR} as the input of the fuzzy controller. As a result, another quantity named the virtual lateral coordinate of ICR Vy_{ICR} is used. This quantity has a linear relationship with the steer angle, and by using equations (2) to (4) changes to y_{ICR}.

$$y_{ICR} = \frac{x_A - x_{ICR}}{\tan \delta_A} + y_A \tag{2}$$

$$Vy_{ICR} = \frac{T_T}{2\delta_{max}} \delta \tag{3}$$

$$y_{ICR} = \frac{L_T}{2tan(\frac{2\delta_{max} Vy_{ICR}}{T_T})} + \frac{T_T}{2} \frac{Vy_{ICR}}{|Vy_{ICR}|} \tag{4}$$

In Figure 3 (a), the diagram of the fuzzy controller for the point (A) is shown. In this controller, the lateral offset of the first point ΔY_A, the variation rate of this offset $\Delta\dot{Y}_A$, and y_{ICR} are fed back as the input. ΔVy_{ICR} is also used as an output.

Figure 3. Fuzzy logic controllers.

In addition to the lateral offset of the first point, the controller should be aware of getting farther or closer to the target path. $\Delta\dot{Y}_A$ is a quantity that can provide this information to the controller.

In designing the controller, creating smooth steering angles with minimum fluctuation should be considered, which is achievable by applying gradual output. Because of this reason, ΔVy_{ICR} is used as the controller's output. In the case of using the lateral coordinate variation as an output, the controller should instantly be aware of previous location of Vy_{ICR}, so a feedback is needed.

Membership functions for the inputs and outputs of first point controller are shown in Figure 4. Vy_{ICR} is divided into three membership functions, {N, Z, P}. When Vy_{ICR} is in zone Z, y_{ICR} is at infinity and the tractor is moving in a straight line, and when it moves toward the negative (positive) zone, y_{ICR} moves from infinty to the right (left) side of tractor. The steering angle also increases and the tractor is moving on a curved path.

Figure 4. Membership functions for the controller (A).

ΔY_A is divided into five membership functions {NB, N, Z, P, PB}. When ΔY_A is located in zone Z, the first point is on the target path, and when it is on the right (left) side, it will be negative (positive). $\Delta\dot{Y}_A$ is divided into three membership functions. When this input is in zone Z, the first point is moving parallel to the target path. According to Figure 5, if ΔY_A is negative (positive), locating $\Delta\dot{Y}_A$ in a negative zone means getting away (approaching to) from the target path. The controller output ΔVy_{ICR} is divided into nine membership functions, {NB, NM, NS, NVS, Z, PVS, PS, PM, PB}, and each of their uses depends on fuzzy rules.

Figure 5. Relationship between a deviation and its derivative according to the target path.

To extract fuzzy rules after determining controller input, if ΔY_A and ΔY_A are located in zone Z, ΔVy_{ICR} is considered zero. Otherwise, depending on the situation, an appropriate quantity will be considered. In case of having a positive lateral offset of the first point ($\Delta Y_A = P$), the decision process will be as following:

- If the lateral offset is increasing ($\Delta \dot{Y}_A = P$), then y_{ICR} will be quickly transferred to the negative side ($\Delta Vy_{ICR} = NB$).
- If the first point is moving parallel to the path ($\Delta \dot{Y}_A = Z$), a minor change in y_{ICR} to the negative side offset will be reduced ($\Delta Vy_{ICR} = NS$).
- If the first point is approaching to the path ($\Delta \dot{Y}_A = N$), there is no need to change y_{ICR} , which means that ($\Delta Vy_{ICR} = Z$).

By adding the input y_{ICR}, the above rules will be changed. By approaching y_{ICR} to the tractor, its rate reduces. In the case of y_{ICR} moving from one side to the other side of axis, the rate increases. The fuzzy rules are represented in Table 2. To increase controller speed in sharp manoeuvres, the weight of ΔY_A in the decision process has increased by using the last row of fuzzy rules in Table 2.

As shown in Figure 3 (b), in the controller design of the point (B), which is the same as the point (A), lateral offset ΔY_B, lateral offset rate $\Delta \dot{Y}_B$, and longitudinal coordinate x_{ICR} as feedback are used.

Table 2. Rules for the controller (A).

Using the same reasoning for the point (A) controller, Δx_{ICR} is used as an output. When y_{ICR} is at infinity (Vy_{ICR} in zero zone), a change in x_{ICR} does not have a significant influence on steering angle. Whereas, by approaching y_{ICR} to the vehicle, more severe steering angles are created. Therefore, to prevent a severe steering angle while y_{ICR} approaches to the vehicle, the amount of fuzzy output controller must be reduced. Due to this problem, Vy_{ICR} is selected as another input.

In Figure 6, all controller inputs consist of three membership functions, {N, Z, P}. Δx_{ICR} as the controller output is divided into nine membership functions {NB, NM, NS, NVS, Z, PVS, PS, PM, PB}.

Figure 6. Membership functions for the controller (B).

The procedure of extracting fuzzy rules for the point (B) is similar to that at point (A), but the difference is that changing longitudinal coordinate of ICR will not always reduce the offset, and in some cases, it can only prevent increasing it. Fuzzy rules of the point (B) are represented in Table 3.

When y_{ICR} is at infinty (Vy_{ICR} in zone Z), a x_{ICR} variation in x_{ICR} does not change the steering angle. Hence, in fuzzy rules, only two membership functions Vy_{ICR} have been studied.

Table 3. Rules for the controller (B).

3.2. Determining steering angle and angular speed of each tractor's wheel

To determining the steering angle of the tractor in the first step, the ICR should be calculated by using equations (5) and (6).

$$x_{ICR}(i+1) = x_{ICR}(i) + \Delta x_{ICR} \quad (5)$$

$$Vy_{ICR}(i+1) = Vy_{ICR}(i) + \Delta Vy_{ICR} \quad (6)$$

In the second step, by using equation (4), Vy_{ICR} converts to y_{ICR}.

Finally, in the third step, based on geometrical equations, the steering angle and turning radii of each wheel can be calculated by substituting the coordinates of each wheel in relation to the geometric centre in equation (7) and equation (8), as shown in Figure 7 (a).

$$\delta_{ij} = \tan^{-1} - \frac{x_{ij} - x_{ICR}}{y_{ij} - y_{ICR}} \quad (7)$$

$$R_{ij} = \sqrt{\left(x_{ij} - x_{ICR}\right)^2 + \left(y_{ij} - y_{ICR}\right)^2} \quad (8)$$

i: Front (F) , Rear (R)

j: Left (L) , Right (R)

Figure 7. Steering angle calculation.

Using Equation (8), the desired angular speed of a wheel is calculated by substituting turning radii of each wheel in equation (9).

$$\omega_{ref_{ij}} = \frac{r_T R_{ij}}{R_a} \qquad (9)$$

In the above equation, R_a is the effective radius of each tyre, and ω_{ref} is the desired angular speed of each wheel.

3.3. Trailer's upper layer controller

The purpose of the fuzzy controller for the trailer is in determining the yaw rate of the trailer in a way that during the manoeuvre, the rear end point of the controller can be located on the target path and it can be followed thoroughly. This yaw rate has been applied in trailer kinematic equations, and based on that, the steering angle of each wheel is calculable.

The fuzzy controller's inputs are a lateral offset of rear end points in relation to the target path (ΔY_C), the angular difference of the tangent line on a target path at the endpoint ($\Delta\Psi$), and the trailer's yaw rate feedback (r_{ST}). To prevent sharp steering angle in trailer, deviations of yaw rate are used as the output. Figure 3 (c) demonstrates the controller diagram.

In Figure 8, ΔY_C and r_{ST} consist of three membership functions, {N, Z, P}, and $\Delta\Psi$ is consist of five membership functions, {NB, N, Z, P, PB}. In this controller, receding or approaching the endpoint of the target path is determined by $\Delta\Psi$. The controller output, Δr_{ST}, is divided into nine membership functions, {NB, NM, NS, NVS, Z, PVS, PS, NM, PB}.

Figure 8. Membership functions for the controller (C).

If ΔY_C and $\Delta\Psi$ are located in zone Z simultaneously, then Δr_{ST} is equal to zero. If ΔY_C is positive, the decision process will be as follows:

- If the endpoint is getting away from target path ($\Delta\Psi = P$), $\Delta \mathrm{r}_{\mathrm{ST}}$ must increase in the positive direction ($\Delta r_{ST} = PB$).
- If the endpoint is moving in parallel to the target path ($\Delta\Psi = Z$), a slight increasing of Δr_{ST} in the positive direction will result in reduction of lateral offset ($\Delta r_{ST} = PS$).

- If the endpoint is approaching to the target path ($\Delta\Psi = N$), there is no need to change r_{ST} ($\Delta r_{ST} = Z$).

Adding r_{ST} to the above fuzzy rules will change the amount of output. If the desired yaw rate and current speed were in the same direction, the controller's output reduces and vice versa. The fuzzy rules are in Table 4.

Table 4. Rules for the controller (C).

3.4. Determining steering angle of trailer's wheels

After determining r_{ST} in each instant by equation (10), this speed is applied to the kinematic equation of the trailer, which is derived based on Figure 7 (b). Then, by applying each wheel coordinate in equation (11) to (14), the steering angle of each wheel is calculated.

$$r_{ST}(i+1) = r_{ST}(i) + \Delta r_{ST} \tag{10}$$

$$(v_{kl})_x = v_{FW}\, cos(\delta_{FW} - \emptyset_{Art}) - \frac{T_{ST} r_{ST}}{2} \tag{11}$$

$$(v_{kl})_y = v_{FW}\, sin(\delta_{FW} - \emptyset_{Art}) - L_{kl} r_{ST} \tag{12}$$

$$v_{kl} = \sqrt{{(v_{kl})_x}^2 + {(v_{kl})_y}^2} \tag{13}$$

$$\delta_{kl} = tan^{-1}\frac{(v_{kl})_y}{(v_{kl})_x} \tag{14}$$

k: Axle Number=3,4,5

l: Left (L), Right (R)

The steering angle rate depends on speed v, which leads to a change in the fuzzy controller's output. If v increases, the output value must reduce to prevent quick controller response, which causes instability. Because of this reason, appropriate gains K_v for fuzzy controller outputs is determined by trial and error method, which is linear to the speed in the range of 1 and 10 km hr^{-1}.

3.5. Lower layer controller

As previously noted and represented in Figure 9 (a), in the lower layer, the PID controller is used to adjust traction and apply the required torque in each wheel. The PID controller adjusts the voltage of the DC motor based on the difference between the current angular speed as feedback and the target speed, which is calculated by equation (9). By adjusting the voltage, the required torque will be applied on each wheel in order to reach the appropriate value of each wheel's rotational speed.

Figure 9. (a) Lower layer controller (b) Scheme of torque transmission.

By defining quantities in Figure 9 (b), equation (15) to (20) expresses mechanical and electrical equations of wheel and motor. Finally, these equations are converted to two differential equations (21) and (22). By modeling these two equations in MATLAB/Simulink software and applying PID controller using trial and error, controller coefficients are determined.

$$J_{eq} = J_W + {\beta_g}^2 J_M \tag{15}$$

$$\omega_M(t) = \beta_g \omega_W(t) \tag{16}$$

$$T_t(t) = \beta_g T_M \tag{17}$$

$$T_M(t) = K_T I(t) \tag{18}$$

$$J_{eq}\dot{\omega_W}(t) = T_t - \beta_g B \omega_W(t) - T_L \tag{19}$$

$$E(t) = RI(t) + L\frac{dI(t)}{dt} + K_B \omega_M(t) \tag{20}$$

In the above equations, J_{eq} is equivalent inertia, J_W is wheel inertia, J_M is motor inertia, β_g is gear ratio to increase torque, ω_M is angular speed of motor, ω_W is angular speed of wheel, T_t is torque on each wheel, T_M is applied torque from motor, T_L is opposing torque, E is potential difference from motor, R is internal resistance of motor, I is current flow, and K_B is Back-EMF constant, B is motor viscous friction constant.

$$\frac{dI}{dt} = \frac{1}{L}\left(E - \beta_g K_B \omega_W - RI\right) \tag{21}$$

$$\frac{d\omega_W}{dt} = \frac{1}{J_{eq}}\left(\beta_g K_T I - \beta_g B \omega_W - T_L\right) \tag{22}$$

4. TYRE MODEL

For the simulation procedure, the internal tyre model of Trucksim software package has been used.[41] The internal tyre models use the tables of shear forces and moments measured in the tests. These forces and moments are defined at the ground, then transmitted and applied at the wheel centre, in order to be used in multi-body dynamic model equations in Trucksim. Like most tyre models, the tyre forces and moments are calculated based on the following kinematical variables: slip angle α, longitudinal slip ratio k, and vertical load F_Z. However, in the internal tyre model these variables are used as inputs for look-up tables instead of equations to obtain the forces and moments. The aforementioned kinematic variables are defined as follows:

Longitudinal slip (k) is defined as:

$$k = \frac{\omega}{\omega_0} - 1 \tag{23}$$

where ω is the angular speed of the wheel, and ω_0 is the zero-slip angular speed of the wheel:

$$\omega_0 = \frac{V_X}{R_{RE}} - 1 \tag{24}$$

where R_{RE} is the effective rolling radius.

The slip angle (α) for each tyre is defined by:

$$\alpha = \tan^{-1}(\frac{V_Y}{V_X}) \tag{25}$$

Where V_X and V_Y are velocity components of wheel centre in the ground plane.

In pure longitudinal and lateral slip F_X, F_Y, and M_Z are calculated based on 2D curves shown in Figure 10 as functions of two independent variables α and k. These tables were drawn for several vertical loads, and the linear interpolation/extrapolation is used for other vertical loads. Therefore, F_X, F_Y, and M_Z can be defined as:

$$\begin{aligned} F_X &= FX(F_Z, k) \qquad \{For\ \alpha = 0\} \\ F_Y &= FY(F_Z, \alpha) \qquad \{For\ k = 0\} \\ M_Y &= MY(F_Z, \alpha) \qquad \{For\ k = 0\} \end{aligned} \tag{26}$$

Figure 10. Shear forces and moments measured in tests - (a) Longitudinal force (b) Lateral force (c) Aligning moment.

For combined situations, using the Pacejka and Sharp's method, the longitudinal and lateral slips are combined to get the total theoretical slip [42].

$$\sigma_{total} = \sqrt{(\sigma_X)^2 + (\sigma_Y)^2} \tag{27}$$

where:

$$\sigma_X = -\frac{k}{k+1}, \qquad \sigma_Y = \frac{\tan(\alpha)}{k+1} \tag{28}$$

The theoretical slips are then normalized by peak slip values, σ_{Xmax} and σ_{Ymax}. Peak slip values are those that cause peak F_X and F_Y. The total normalized slip is:

$$\grave{\sigma}_{total} = \sqrt{(\grave{\sigma}_X)^2 + (\grave{\sigma}_Y)^2} \tag{29}$$

where:

$$\grave{\sigma}_X = \frac{\sigma_X}{\sigma_{Xmax}}, \qquad \grave{\sigma}_Y = \frac{\sigma_Y}{\sigma_{Ymax}} \tag{30}$$

The equivalent longitudinal and lateral slips are calculated from the normalized total theoretical slip:

$$\grave{k} = \frac{\grave{\sigma}_{total}.\sigma_{Xmax}.sign(\sigma_X)}{1 + \grave{\sigma}_{total}.\sigma_{Xmax}.sign(\sigma_X)}, \qquad \grave{\alpha} = \tan^{-1}(\grave{\sigma}_{total}.\sigma_{Ymax}.sign(\sigma_Y)) \tag{31}$$

Using the equivalent longitudinal and lateral slips, the so-called “base-curves” are obtained by means of linear interpolation of the tabular data. Based on the Pacejka and Sharp’s method, the normalized slip values are modified to include the friction ratio since the friction coefficient of measurements is different from the friction coefficient of the simulation.

$$F_{X0} = FX\left(F_Z, \frac{\mu_0}{\mu}\grave{k}\right), \qquad F_{Y0} = FY\left(F_Z, \frac{\mu_0}{\mu}\grave{\alpha}\right) \tag{32}$$

The base-curves are then modified in order to account for the anisotropic properties of the tyre-road friction.

$$\grave{F}_{X0} = F_{X0} - \varepsilon(F_{X0} - F_{Y0})\left(\frac{\grave{\sigma}_Y}{\grave{\sigma}_{total}}\right)^2, \qquad \grave{F}_{Y0} = F_{Y0} - \varepsilon(F_{Y0} - F_{X0})\left(\frac{\grave{\sigma}_X}{\grave{\sigma}_{total}}\right)^2 \tag{33}$$

where $\varepsilon = \grave{\sigma}_{total}$ for $\grave{\sigma}_{total} < 1$ and $\varepsilon = 1$ for $\grave{\sigma}_{total} > 1$.

The moment and forces are finally calculated by:

$$\begin{aligned} F_X &= \grave{F}_{X0}\frac{\mu}{\mu_0}\frac{\sigma_X}{\sigma_{total}} \\ F_Y &= \grave{F}_{Y0}\frac{\mu}{\mu_0}\frac{\sigma_Y}{\sigma_{total}} \\ M_Z &= \frac{MZ(F_Z, \grave{\alpha})}{F_{Y0}}|F_Y| \end{aligned} \tag{34}$$

Various methods have been proposed to analyze the transient behaviour of tyre, due to its deformable structure [43, 44]. The tyre model used in this manuscript is based on a concept known as *relaxation length*, described by Bernard and Clover [45].

5. RESULTS AND DISCUSSION

In order to evaluate the tractor and trailer's wheels' steering performance as well as controller performance, a computer simulation has been carried out. For this simulation, the controller has been implemented in MATLAB/Simulink software [46]. For the vehicle dynamic model and active behavior analysis, Trucksim software has been used [41].

In order to show the effectiveness of the suggested controller in reducing off-tracking of point B and C, the behavior of automatic steering tractor semi-trailers is compared back to back with:

1. A conventional tractor and semi-trailer
2. A conventional tractor semi-trailer with the control structure represented in reference [25].

Here, the former is named *conventional*, the latter is named *CT-AT*, and the studied vehicle is named *AWS*. It is noted that only the performance of path tracking in these vehicles has been evaluated. The performances have been compared in *roundabout* and *sharp 90 degree* tests. The former is the standard test in low speed and the latter is not standard but an extreme manoeuvre, which is considered to be a challenge for the conventional vehicles. The aim of comparing CT-AT and AWS is to analyze the effect of steerability on off tracking rather than the proposed algorithm itself. It should be noted that through the manoeuvres covered by CT-AT, the conventional steering angle is adjusted in a way that the first point of the tractor will be located on the target path; whereas, AWS determines steering angles automatically, only by using offset of first and second points of tractor.

Features of the simulated vehicle are represented in Table 5.

Table 5. Vehicle specificatios

5.1. Roundabout test

In this standard manoeuvre, the vehicle covers a straight line with a constant speed 10 km hr^{-1}, and then, it enters the round section and after 450 degrees turning, it comes out on the straight line. The front end point in this manoeuvre moves on a circle with radius of 11.25 m. The target path of front end point of tractor is shown on Figure 11. This figure also shows the AWS vehicle thorough the manoeuvre in shaded shape.

Figure 10. Roundabout manoeuvre path.

According to Figure 12 (a), the front end point has passed the target path well. Additionally, the controller has been able to reduce the rear end point offset considerably. As shown in this figure, the front end point and rear endpoint offsets happened during a quick change of steering angles when vehicle enters and exits the round path, which proves that controller has been able to control the vehicle on the target path. For CT-AT, the steering angle of the tractor is defined in a way that the front end of the tractor exactly passes the desired path. Therefore, it has not been compered in simulation results. In Figure 12 (b), although third point offset reduced considerably by CT-AT vehicle, the control system in the AWS vehicle has been able to almost eliminate it.

Generated lateral forces in the tyres of tractor and trailer wheels, which are representative of sideslip angles, have been compared for all three mentioned vehicles in Figure 12 (e), (f) and (g). As shown, the CT-AT vehicle has a significant effect on the generated force in the trailer's wheels, and while it has reduced tyre wear, these forces are still high in axles 4 and 5; whereas, the AWS vehicle has been able to further reduce lateral forces of trailer wheels and minimize them.

As shown in Figure 12 (c), the front axle's steering angle of the AWS vehicle has been reduced to half compared to the conventional vehicle due to steerability of vehicle rear wheels. Also, the summation of the applied steering angles has slightly decreased. Moreover, in Figure 12 (d), although the maximum angle in AWS trailer's wheels has been increased compared to CT-AT, the summation of applied steering angles has not changed. This shows that the change in the control effort is negligible.

Figure 12. Simulation results of the roundabout manoeuvre

5.2. Sharp 90 degree test

In order to challenge the new capabilities of AWS vehicle and its controller, sharp 90 degree test has been designed as an extreme manoeuvre to check the controller's performance in sharp intersections. In this manoeuvre, the vehicle goes by constant speed of 1 km hr^{-1} from straight path to a circle path by radius of 2.5 meters, and after passing 90 degrees turning, it exits in a straight line as shown in Figure 13.

Figure 13. 90 degrees manoeuvre path.

As shown in Figure 14 (a), the conventional tractor has a large offset because of its limitation in steering angle. Whereas, the AWS vehicle has eliminated the first point's offset and has substantially reduced second point offset. Also, In Figure 14 (b), off-tracking of the AWS trailer is negligible to conventional. In CT-AT, however, there is significant reduction and off-tracking is still not in the accepted range.

In this manoeuvre, the lateral force of the trailer's wheels is reduced in the AWS vehicle, shown in Figure 14 (e). However, the lateral force of the tractor's rear axle wheels (Axle 2 in the figure) increased because of the applied steering angle.

As shown in Figure 14 (c) and (d), in this manoeuvre, the steering angle of the conventional tractor (Axle 1 in the figure) will be at its maximum and it will increase the first point's offset from the target path. Due to the wide range of steerability in the AWS tractor, the steering angle can be increased to reduce the offset effectively as well. Table 6 summarizes off tracking, lateral forces, and the steering angle of all the three vehicles in both manoeuvres.

Figure 14. Simulation results of the 90 degrees manoeuvre.

Table 6. Summary of simulations results

6. CONCLUSION

In this manuscript, the effect of an automated steering articulated vehicle with an all-wheel steering system has been investigated. All wheels of the tractor and trailer are steerable; whereas, the wheels of the tractor are also equipped with independent traction control. The controllers of the tractor and trailer are operating independently in two layers. A fuzzy controller in the upper layer reduces the off tracking by determining the instant centre of rotation in its unit. It uses a lateral offset of three predefined points and corresponding rate as its inputs. Having the instant centre of rotation of each unit, the steering angle of it can be determined using kinematic relationships. In the lower layer, a PID controller tunes the steering angle of each wheel as well as the applied torque. The overall purpose of this system is to regulate the steering angle of all wheels such that the end point of tractor and trailer follow the desired path, which is the initial path of truck's first point. The simulated manoeuvres in TruckSim software show that by using an independently controlled all wheel steering system in an articulated vehicle, the off tracking in both tractor and trailer even in very sharp curves can be reduced. Additionally, it has been shown that although the lateral forces in CT-AT vehicle have decreased when compared to conventional vehicles, the AWS system can significantly mitigate them on top of aforementioned capabilities. Moreover, the hierarchical controller can effectively control the speed and steering angle of wheels.

REFERENCES

1. Xiong B and Qu S. Intelligent Vehicle's Path Tracking Based on Fuzzy Control. *Journal of transportation systems engineering and information technology*. 2010; 10: 70-5.
2. Tsui W, Masmoudi MS, Karray F, Song I and Masmoudi M. Soft-computing-based embedded design of an intelligent wall/lane-following vehicle. *Mechatronics, IEEE/ASME Transactions on*. 2008; 13: 125-35.
3. Goodarzi A, Sabooteh A and Esmailzadeh E. Automatic path control based on integrated steering and external yaw-moment control. *Proceedings of the Institution of Mechanical Engineers, Part K: Journal of multi-body dynamics*. 2008; 222: 189-200.
4. Goodarzi A and Ghajar M. Integrating lane-keeping system with direct yaw moment control tasks in a novel driver assistance system. *Proceedings of the Institution of Mechanical Engineers, Part K: Journal of multi-body dynamics*. 2014: 1464419314545408.
5. Zobel D and Weyand C. On the maneuverability of heavy goods vehicles. IEEE, 2008, p. 2303-8.
6. Bolzern P, DeSantis RM, Locatelli A and Masciocchi D. Path-tracking for articulated vehicles with off-axle hitching. *Control Systems Technology, IEEE Transactions on*. 1998; 6: 515-23.
7. Rangavajhula K and Tsao HSJ. Active trailer steering control of an articulated system with a tractor and three full trailers for tractor-track following. *International Journal of Heavy Vehicle Systems*. 2007; 14: 271-93.
8. Bennett S. *Heavy duty truck systems*. Delmar Pub, 2010.
9. Jujnovich B, Odhams C, Roebuck R and Cebon D. IMPLEMENTATION OF ACTIVE REAR STEERING OF A TRACTOR–SEMI-TRAILER. 2008.
10. Pflug HC and von Glasner E. Commercial Vehicles with Intelligent Rear Axle Steering Systems. Society of Automotive Engineers, 400 Commonwealth Dr, Warrendale, PA, 15096, USA, 1996.
11. Choi MW, Park JS, Lee BS and Lee MH. The performance of independent wheels steering vehicle (4WS) applied Ackerman geometry. IEEE, 2008, p. 197-202.
12. Jujnovich B and Cebon D. Comparative performance of semi-trailer steering systems. 2002, p. 16-20.
13. Lee JH, Chung W, Kim M and Song JB. A passive multiple trailer system with off-axle hitching. *INTERNATIONAL JOURNAL OF CONTROL AUTOMATION AND SYSTEMS*. 2004; 2: 289-97.
14. Prem H, Ramsay E, McLean J, Pearson R, Woodrooffe J and de Pont J. Definition of potential performance measures and initial standards. *National Road Transport Commission Discussion Paper 81p*. 2001.
15. Jujnovich B and Cebon D. Validation of a semi-trailer steering model. 2004.
16. Sweatman P, Atley K and O'Reagon J. Trial Assessment of Stearable Axle System. 2004, p. 45-55.
17. Islam MM and He Y. An Optimal Preview Controller for Active Trailer Steering Systems of Articulated Heavy Vehicles. SAE Technical Paper, 2011.
18. Cheng C and Cebon D. Improving roll stability of articulated heavy vehicles using active semi-trailer steering. *Vehicle System Dynamics*. 2008; 46: 373-88.
19. Cheng C, Roebuck R, Odhams A and Cebon D. High-speed optimal steering of a tractor–semitrailer. *Vehicle System Dynamics*. 2011; 49: 561-93.
20. Lin X, Ding N, Xu G and Gao F. High Speed Optimal Yaw Stability of Tractor-Semitrailers with Active Trailer Steering. SAE Technical Paper, 2014.
21. He Y and Islam MM. An automated design method for active trailer steering systems of articulated heavy vehicles. *Journal of Mechanical Design*. 2012; 134: 041002.
22. Fancher P and Winkler C. Directional performance issues in evaluation and design of articulated heavy vehicles. *Vehicle System Dynamics*. 2007; 45: 607-47.
23. Notsu I, Takahashi S and Watanabe Y. Investigation into turning behavior of semi-trailer with additional trailer-wheel steering--a control method for trailer-wheel steering to minimize trailer rear-overhang swing in short turns. SAE Technical Paper, 1991.
24. Odhams A, Roebuck R, Cebon D and Winkler C. Dynamic safety of active trailer steering systems. *Proceedings of the Institution of Mechanical Engineers, Part K: Journal of multi-body dynamics*. 2008; 222: 367-80.
25. Odhams A, Roebuck R, Jujnovich B and Cebon D. Active steering of a tractor–semi-trailer. *Proceedings of the Institution of Mechanical Engineers, Part D: Journal of Automobile Engineering*. 2011; 225: 847-69.
26. Oreh ST, Kazemi R and Azadi S. A new desired articulation angle for directional control of articulated vehicles. *Proceedings of the Institution of Mechanical Engineers, Part K: Journal of multi-body dynamics*. 2012: 1464419312445426.
27. Shida M. Development of integerated vehicle control system of 'Fine-X' which realized freer movment. *The 8th International Symposium on Advanced Vehicle Control*. AVEC062006.
28. Lam TL, Qian H and Xu Y. Omnidirectional steering interface and control for a four-wheel independent steering vehicle. *Mechatronics, IEEE/ASME Transactions on*. 2010; 15: 329-38.

29. Brembeck J, Ho LM, Schaub A, Satzger C and Hirzinger P. ROMO–the robotic electric vehicle. *IAVSD, Aug*. 2011: 14-9.
30. Wu SJ, Chiang HH, Perng JW, Lee TT and Chen CJ. The automated lane-keeping design for an intelligent vehicle. IEEE, 2005, p. 508-13.
31. Kodagoda K, Wijesoma W and Teoh E. Fuzzy speed and steering control of an AGV. *Control Systems Technology, IEEE Transactions on*. 2002; 10: 112-20.
32. Hiraoka T, Nishihara O and Kumamoto H. Automatic path-tracking controller of a four-wheel steering vehicle. *Vehicle System Dynamics*. 2009; 47: 1205-27.
33. Raksincharoensak P, Nagai M and Mouri H. Investigation of automatic path tracking control using four-wheel steering vehicle. *Vehicle Electronics Conference, 2001 IVEC 2001 Proceedings of the IEEE International*. IEEE, 2001, p. 73-7.
34. Marumo Y, Mouri H, Wang Y, Kamada T and Nagai M. Study on automatic path tracking using virtual point regulator. *JSAE review*. 2000; 21: 523-8.
35. Song Y-D, Chen H-N and Li D-Y. Virtual-point-based fault-tolerant lateral and longitudinal control of 4W-steering vehicles. *Intelligent Transportation Systems, IEEE Transactions on*. 2011; 12: 1343-51.
36. Bunte T, Brembeck J and Ho LM. Human machine interface concept for interactive motion control of a highly maneuverable robotic vehicle. IEEE, 2011, p. 1170-5.
37. Bakker T, van Asselt K, Bontsema J, Müller J and van Straten G. A path following algorithm for mobile robots. *Autonomous Robots*. 2010; 29: 85-97.
38. Antonelli G, Chiaverini S and Fusco G. A fuzzy-logic-based approach for mobile robot path tracking. *Fuzzy Systems, IEEE Transactions on*. 2007; 15: 211-21.
39. Zhong T and Qiu M. Fuzzy Control of Intelligent Vehicle Based on Visual Navigation System. 2010, p. 97.
40. Zimic N and Mraz M. Decomposition of a complex fuzzy controller for the truck-and-trailer reverse parking problem. *Mathematical and computer modelling*. 2006; 43: 632-45.
41. Mechanical Simulation, TruckSim 8.0, Documentation and Help. 2009.
42. Pacejka HB and Sharp RS. Shear force development by pneumatic tyres in steady state conditions: a review of modelling aspects. *Vehicle System Dynamics*. 1991; 20: 121-75.
43. Mastinu G, Gaiazzi S, Montanaro F and Pirola D. A semi-analytical tyre model for steady-and transient-state simulations. *Vehicle System Dynamics*. 1997; 27: 2-21.
44. Mavros G, Rahnejat H and King P. Analysis of the transient handling properties of a tyre, based on the coupling of a flexible carcass—belt model with a separate tread incorporating transient viscoelastic frictional properties. *Vehicle System Dynamics*. 2005; 43: 199-208.
45. Bernard JE and Clover CL. Tire modeling for low-speed and high-speed calculations. SAE Technical Paper, 1995.
46. Mathworks, MATLAB 7.1, Documentation and Help, Fuzzy Logic Toolbox. 2010.

NOMENCLATURE

To avoid a large list, the parametric values are denoted by $**$ sign.

$\dot{**}$	Derivative of variable
$\hat{**}$	Estimated value of variable
$**_{A/B/C/ICR}$	Variable related to point A / B / C / ICR
$**_{FW}$	Variable related to fifth wheel
$**_{P}$	Variable related to path
$**_{ST}$	Variable related to semi-trailer
$**_{T}$	Variable related to tractor
$\Delta\,**$	Variation of variable
B	Viscous friction constant
E	Potential difference
F_X	Longitudinal tyre force
F_Y	Lateral tyre force
FOH	Front overhang of tractor

HDB	Distance between fifth wheel and front axle of tractor (Hitch Dist. Back)
I	Electric current
J_{eq}	Equivalent Inertia
J_M	Inertia of motor
J_W	Inertia of wheel
k	Longitudinal slip
K_B	Back-EMF constant
K_T	Torque constant
L	Inductance of motor
L_C	Distance between fifth wheel and end of semi-trailer
L_T	Wheelbase of tractor
M_Z	Aligning moment
R	Internal resistance of motor
R_{**}	Turning radius of a point on vehicle
R_{RE}	Effective rolling radius
r	Yaw rate
S	Distance that a point has passed
T_L	Opposing torque
T_t	Torque on wheel
T_M	Applied torque from motor
T_t	Torque on wheel
u	Longitudinal velocity
v	Velocity
Vy_{ICR}	Virtual lateral coordinate of ICR
X_{**}, Y_{**}	Coordinate in global coordinate system
x_{**}, y_{**}	Coordinate in vehicle coordinate system
x_{ICR}, y_{ICR}	Coordinate of ICR in vehicle coordinate system
α	Slip Angle
β_g	Gear Ratio
Δr_{ST}	Yaw rate variation of semi-trailer
$\Delta x_{ICR}, \Delta y_{ICR}$	Coordinate variation of ICR
δ	Steer angle
δ_{max}	Maximum possible steer angle
λ	Speed angle in global coordinate
μ	Friction coefficient in measurement
μ_0	Friction coefficient in simulation
$\emptyset_{Art}$	Articulation angle
ψ	Yaw angle
ω_0	Zero-Slip angular speed of wheel
ω_M	Angular speed of motor
ω_{ref}	The desired angular speed of wheel
ω_W	Angular speed of wheel

ABBREVIATION

AWS	All Wheel Steer
CT-AT	Conventional Tractor-Active Trailer
ICR	Instance Centre of Rotation

APPENDIX A: Kinematic Model Derivation

Figure 15. Parameter definition of (a) tractor and (b) tractor estimator.

Figure 16. Parameter definition of (a) trailer and (b) trailer estimator.

An estimator is an imaginary vehicle, which moves by the real vehicle while points (A), (B) and (C) are on the target path. First, to create this estimator, the target path in the global coordinate system should be determined, which point $A((\mathrm{X_P})_\mathrm{A}, (\mathrm{Y_P})_\mathrm{A})$ is passing through. This issue is possible, as shown in Figure 15 (a) and equations (35) to (39). According to equation (35), the lateral and longitudinal coordinates of (A) can be derived based on time integration from components of the vehicle's speed in X and Y directions.

$$X_A = \int_0^t \frac{u}{cos(\delta_A)} cos(\psi_T + \delta_A)dt \text{ , and}$$
$$Y_A = \int_0^t \frac{u}{cos(\delta_A)} sin(\psi_T + \delta_A)dt \tag{35}$$

where, δ_A is the speed angle of point (A) with respect to longitudinal direction of tractor, which is the resultant of equation (36).

$$\delta_A = \tan^{-1} \frac{(x_A)_T - (x_{ICR})_T}{(y_{ICR})_T} \dagger \tag{36}$$

Now, by substituting the derived parameters from equations (35) in equation (37), the coordinates of target path can be determined.

$$(X_P)_A = X_A + \Delta Y_A sin(\psi_P) \text{, and}$$
$$(Y_P)_A = Y_A - \Delta Y_A cos(\psi_P) \tag{37}$$

ψ_P must be calculated from equations (38) and (39).

$$\psi_P = \tan^{-1} \frac{(v_P)_Y}{(v_P)_X} \tag{38}$$

$$(v_P)_X = \frac{d(X_P)_t}{dt} \text{, and}$$
$$(v_P)_Y = \frac{d(Y_P)_t}{dt} \tag{39}$$

After determining the desired path coordinates in global coordinate system, a lookup table is created. This table is based on 1: The distance that the front end point on the tractor estimator (A) has passed $\acute{S}_A$ acts as an input, and the speed angle of this point in relation to the global coordinate system $\acute{\lambda}_A$, and 2: the lateral coordinate

† Subuscript (T) and (ST) are respectively representative of tractor and semi-trailer coordinate systems

$(\mathrm{Y}_P)_A$ and longitudinal coordinate $(\mathrm{X}_P)_A$ of the target path in the global coordinate system act as outputs. The process is the same for points (B) and (C). Thus, by entering ($\acute{S_B}$ and $\acute{S_C}$) in the table, $\acute{\lambda}_B$, $\acute{\lambda}_c$, $(\mathrm{Y}_P)_{B,C}$ and $(\mathrm{X}_P)_{B,C}$ can be determined. Through the manoeuvre, the table's information will be entered actively, updated instantly, and saved in the memory. According to the Figure 15 (b), which is the tractor estimator and by using equations (39) to (42), $\acute{S_A}$, $(\mathrm{X}_P)_A$ and $(\mathrm{Y}_P)_A$ can be determined and then complete the table. In the equations estimator, the parameters have prim script.

$$(\acute{v_A})_X = (v_P)_X \text{ , and} \qquad (\acute{v_A})_Y = (v_P)_Y \tag{40}$$

$$\acute{v}_A = \sqrt{((\acute{v_A})_Y)^2 + ((\acute{v_A})_X)^2} \tag{41}$$

$$\acute{S_A} = \int_0^t \acute{v}_A dt \tag{42}$$

To determine ($\acute{S_B}$), based on the Figure 15 (b), equations (43) to (49) are used. By entering $\acute{S_B}$ in the lookup table, target coordinates of point B ($(\mathrm{X}_P)_B, (\mathrm{Y}_P)_B$) are extractable.

$$\acute{S_B} = \int_0^t \acute{v}_B dt - OL \tag{43}$$

$$\acute{v}_B = \acute{R}_B \acute{r}_T \tag{44}$$

$$\acute{r}_T = \frac{\acute{v}_A}{\acute{R}_A} \tag{45}$$

The turning radius of points (A) and (B) are determined from equations (46) and (47).

$$\acute{R}_B = \frac{OL\, sin(90 - \acute{\delta_A})}{sin(\acute{\delta_A} - \acute{\delta_B})} \tag{46}$$

$$\acute{R}_A = \frac{OL\, sin(90 + \acute{\delta_B})}{sin(\acute{\delta_A} - \acute{\delta_B})} \tag{47}$$

$$\acute{\delta_{A(B)}} = \acute{\lambda}_{A(B)} - \acute{\psi}_T \tag{48}$$

$$\acute{\psi}_T = tan^{-1}\frac{((Y_P)_A - (Y_P)_B)}{((X_P)_A - (X_P)_B)} \tag{49}$$

To determine the current coordinates of (B), equations (50) to (56) are used. Hence, by comparing current and target points coordinate, the offset of point (B) can be calculated.

The turning radii of A and B are calculated via equations (50) and (51), and then, the yaw rate of the vehicle is determined with equations (52) and (53).

$$R_A = \sqrt{(x_A - x_{ICR})^2 + (y_{ICR})^2} \tag{50}$$

$$R_B = \sqrt{(x_B - x_{ICR})^2 + (y_{ICR})^2} \tag{51}$$

$$r_T = \frac{v_A}{R_A} \tag{52}$$

$$v_A = \frac{u}{\cos(\delta_A)} \tag{53}$$

By substituting these parameters in equation (54), the speed of point (B) and its angle w.r.t. longitudinal coordinates of vehicle can be found.

$$\delta_B = \tan^{-1}\frac{(x_B)_T - (x_{ICR})_T}{(y_{ICR})_T}, \text{and } v_B = R_B r_T \tag{54}$$

Now, by substituting δ_B and v_B in equations (55) and (56), the coordinates of pint B in the global coordinate system can be determined.

$$\mathrm{X}_B = \int_0^t (v_B \cos(\delta_B + \psi_T))dt - OL \tag{55}$$

$$\mathrm{Y}_B = \int_0^t (v_B \sin(\delta_B + \psi_T))dt \tag{56}$$

According to Figure 16 (a) and equations (57) to (64), $X_C\ and\ Y_C$ are calculable and are used to determine the target end point value of trailer estimator. By using equations (57) to (59), the speed and speed angle of fifth wheel w.r.t longitudinal axis of tractor can be found.

$$R_{FW} = \sqrt{((x_{FW})_T - (x_{ICR})_T)^2 + (y_{ICR})_T{}^2} \tag{57}$$

$$v_{FW} = R_{FW} r_T \tag{58}$$

$$\delta_{FW} = \tan^{-1}\frac{(x_{FW})_T - (x_{ICR})_T}{(y_{ICR})_T} \tag{59}$$

By calculating the angle between the tractor and the trailer ($\emptyset_{Art}$) through equation (60) and substituting the parameter from equation (61) to equations (62) and (63), the component of speed of point (C), amount and its angle w.r.t to trailer's longitudinal axis are quantifiable.

$$\emptyset_{Art} = \psi_{ST} - \psi_T \tag{60}$$

$$((v_C)_x)_{ST} = v_{FW}\cos(\delta_{FW} - \emptyset_{Art}), \text{and } \left((v_C)_y\right)_{ST} = v_{FW}\sin(\delta_{FW} - \emptyset_{Art}) - L_C r_{ST} \tag{61}$$

$$v_C = \sqrt{((v_C)_x)_{ST}{}^2 + \left((v_C)_y\right)_{ST}{}^2} \tag{62}$$

$$\delta_C = \tan^{-1}\frac{\left((v_C)_y\right)_{ST}}{((v_C)_x)_{ST}} \tag{63}$$

Now, the components of coordinates of point (C), in global coordinate system can be determined, using equation (64).

$$X_C = \int_0^t v_C cos(\psi_{ST} + \delta_C)\, dt \text{ , and}$$

$$Y_C = \int_0^t v_C cos(\psi_{ST} + \delta_C)\, dt \tag{64}$$

In a similar manner to that of the tractor estimator, the trailer estimator consists of kinematic equations, which are determined by having the rear end point of trailer on target path and pivot point of tractor estimator. In equations (65) to (76) and Figure 16 (b), by entering $\acute{S_C}$ in the mentioned look up table, $\acute{\lambda}_C$, $(\mathrm{Y}_P)_C$ and $(\mathrm{X}_P)_C$ can be calculated in the global coordinate system, and by having this coordinate and current coordinate, the lateral offset is measurable. The lateral and longitudinal global coordinates of the fifth wheel are calculated using equations (65) to (67).

$$(X_P)_{FW} = \frac{OL-L_H}{OL}((X_P)_A - (X_P)_B) + (X_P)_B,\ and$$

$$(Y_P)_{FW} = \frac{OL-L_H}{OL}((Y_P)_A - (Y_P)_B) + (Y_P)_B \tag{65}$$

$$\acute{\delta_C} = \acute{\lambda}_C - \acute{\psi}_{ST} \tag{66}$$

$$L_H = HDB + FOH \tag{67}$$

By substituting the coordinates of fifth wheel in equations (68), the trailer's turning radius and yaw rate can be derived from equations (69) to (74).

$$\acute{\psi}_{ST} = \tan^{-1}\frac{((\mathrm{Y}_P)_{FW} - (\mathrm{Y}_P)_C)}{((\mathrm{X}_P)_{FW} - (\mathrm{X}_P)_C)} \tag{68}$$

$$\acute{r}_{ST} = \frac{\acute{v}_{FW}}{(\acute{R}_{FW})_{ST}} \tag{69}$$

$$\acute{v}_{FW} = \acute{r}_T \acute{R}_{FW} \tag{70}$$

$$\acute{R}_{FW} = \sqrt{\left(\acute{R}_A\right)^2 + (\mathrm{L}_H)^2 - 2\acute{R}_A \mathrm{L}_H \cos\left(90 - \acute{\delta_A}\right)} \tag{71}$$

$$(\acute{R}_{FW})_{ST} = \frac{L_C.\sin(90 - (\acute{\delta}_{FW} - \acute{\emptyset}_{Art}))}{\sin((\acute{\delta}_{FW} - \acute{\emptyset}_{Art}) - \acute{\delta_C})} \tag{72}$$

$$\acute{\delta}_{FW} = \cos^{-1}\left(\frac{\acute{R}_A \cos(\acute{\delta_A})}{\acute{R}_{FW}}\right) \tag{73}$$

$$\acute{\emptyset}_{Art} = \acute{\psi}_{ST} - \acute{\psi}_{T} \tag{74}$$

Now, by determining the speed of point (C) using equation (75), and integrating it in equation (76), the distanced traveled by point C can be defined.

$$\acute{v}_{C} = \acute{R}_{C}\acute{r}_{ST} \tag{75}$$

$$\acute{S}_{C} = \int_{0}^{t} \acute{v}_{C} dt - (\mathrm{L}_{H} + L_{C}) \tag{76}$$

List of Tables

Table 1. Lingustic terms definition

NB	Negative Big	PB	Positive Big
NM	Negative Medium	PM	Positive Medium
NS	Negative Small	PS	Positive Small
NVS	Negative Very Small	PVS	Positive Very Small
Z	Zero		

Table 2. Rules for the controller (A)

Vy_{ICR}	ΔY_A	$\Delta \dot{Y}_A$	ΔVy_{ICR}	Vy_{ICR}	ΔY_A	$\Delta \dot{Y}_A$	ΔVy_{ICR}	Vy_{ICR}	ΔY_A	$\Delta \dot{Y}_A$	ΔVy_{ICR}
N	NS	N	PM	Z	NS	N	PB	P	NS	N	PS
N	NS	Z	PVS	Z	NS	Z	PS	P	NS	Z	Z
N	NS	P	Z	Z	NS	P	Z	P	NS	P	NS
N	Z	N	PVS	Z	Z	N	PS	P	Z	N	PVS
N	Z	Z	Z	Z	Z	Z	Z	P	Z	Z	Z
N	Z	P	NS	Z	Z	P	NS	P	Z	P	NVS
N	PS	N	PS	Z	PS	N	Z	P	PS	N	Z
N	PS	Z	Z	Z	PS	Z	NS	P	PS	Z	NVS
N	PS	P	NS	Z	PS	P	NB	P	PS	P	NM
----	NB	----	NB	----	PB	----	PB				

Table 3. Rules for the controller (B)

Vy_{ICR}	x_{ICR}	ΔY_B	$\Delta \dot{Y}_B$	Δx_{ICR}	Vy_{ICR}	x_{ICR}	ΔY_B	$\Delta \dot{Y}_B$	Δx_{ICR}	Vy_{ICR}	x_{ICR}	ΔY_B	$\Delta \dot{Y}_B$	Δx_{ICR}
N	N	N	N	PM	N	Z	N	N	PS	N	P	N	N	PVS
N	N	N	Z	PS	N	Z	N	Z	Z	N	P	N	Z	Z
N	N	N	P	PVS	N	Z	N	P	NS	N	P	N	P	NVS
N	N	Z	N	PB	N	Z	Z	N	PVS	N	P	Z	N	Z
N	N	Z	Z	PVS	N	Z	Z	Z	NVS	N	P	Z	Z	Z
N	N	Z	P	NVS	N	Z	Z	P	NB	N	P	Z	P	Z
N	N	P	N	NVS	N	Z	P	N	NVS	N	P	P	N	NVS
N	N	P	Z	NVS	N	Z	P	Z	NVS	N	P	P	Z	NM
N	N	P	P	NS	N	Z	P	P	NS	N	P	P	P	NB
P	N	N	N	NS	P	Z	N	N	NVS	P	P	N	N	NS
P	N	N	Z	Z	P	Z	N	Z	NVS	P	P	N	Z	NM
P	N	N	P	PS	P	Z	N	P	NS	P	P	N	P	NB
P	N	Z	N	NS	P	Z	Z	N	Z	P	P	Z	N	Z
P	N	Z	Z	PVS	P	Z	Z	Z	Z	P	P	Z	Z	Z
P	N	Z	P	PB	P	Z	Z	P	PVS	P	P	Z	P	Z
P	N	P	N	PVS	P	Z	P	N	PVS	P	P	P	N	NM
P	N	P	Z	PM	P	Z	P	Z	PVS	P	P	P	Z	NVS
P	N	P	P	PB	P	Z	P	P	PS	P	P	P	P	PVS

Table 4. Rules for the controller (C)

r_T	ΔY_C	$\Delta\Psi$	Δr_T	r_T	ΔY_C	$\Delta\Psi$	Δr_T	r_T	ΔY_C	$\Delta\Psi$	Δr_T
N	NS	N	NM	Z	NS	N	NS	P	NS	N	NS
N	NS	Z	NVS	Z	NS	Z	NVS	P	NS	Z	NVS
N	NS	P	Z	Z	NS	P	Z	P	NS	P	Z
N	Z	N	NVS	Z	Z	N	NS	P	Z	N	NS
N	Z	Z	Z	Z	Z	Z	Z	P	Z	Z	Z
N	Z	P	PS	Z	Z	P	PS	P	Z	P	PVS
N	PS	N	Z	Z	PS	N	Z	P	PS	N	Z
N	PS	Z	PVS	Z	PS	Z	PVS	P	PS	Z	PVS
N	PS	P	PS	Z	PS	P	PS	P	PS	P	PM
----	----	NB	NB	----	----	PB	PB				

Table 5. Vehicle specificatios

Tractor 2A		Trailer 3A	
Wheelbase	3.7 (m)	Wheelbase	7.7 (m)
Front Overhange	1 (m)	Tandem Axle Spread	1.3 (m)
Rear Overhange	0.5 (m)	Rear Overhange	3 (m)
Track	2.03 (m)	Track	1.82 (m)
Tyre	Internal Model	Tyre	Internal Model
Load on Axle 1	6000 (kg)	Load on Axle 1	7500 (kg)
Load on Axle 2	10000 (kg)	Load on Axle 2	8000 (kg)
Hitch Dist.back	3.1 (m)	Load on Axle 3	8500 (kg)

Table 6. Summary of simulations results

Roundabout	Off-Tracking$_{max}$	Steer Angle$_{max}$	Lateral Tyre Force$_{max}$
Conventional Tractor	1.05 (m)	22 (deg)	10 (KN) with Conventional Trailer 4 (KN) with CT-AT Trailer
AWS Tractor	0.2 (m)	13 (deg)	6.5 (KN)
Conventional Trailer	3.9 (m)	0 (deg)	41.5 (KN)
CT-AT Trailer	0.95 (m)	22 (deg)	11.5 (KN)
AWS Trailer	0.2 (m)	25 (deg)	5 (KN)
Sharp 90 degrees	**Off-Tracking$_{max}$**	**Steer Angle$_{max}$**	**Lateral Tyre Force$_{max}$**
Conventional Tractor	2.5 (m)	40 (deg)	12 (KN) with Conventional Trailer 4 (KN) with CT-AT Trailer
AWS Tractor	0.7 (m)	70 (deg)	16 (KN)
Conventional Trailer	4.3 (m)	0 (deg)	47 (KN)
CT-AT Trailer	1.35 (m)	50 (deg)	22 (KN)
AWS Trailer	0.2 (m)	70 (deg)	4 (KN)

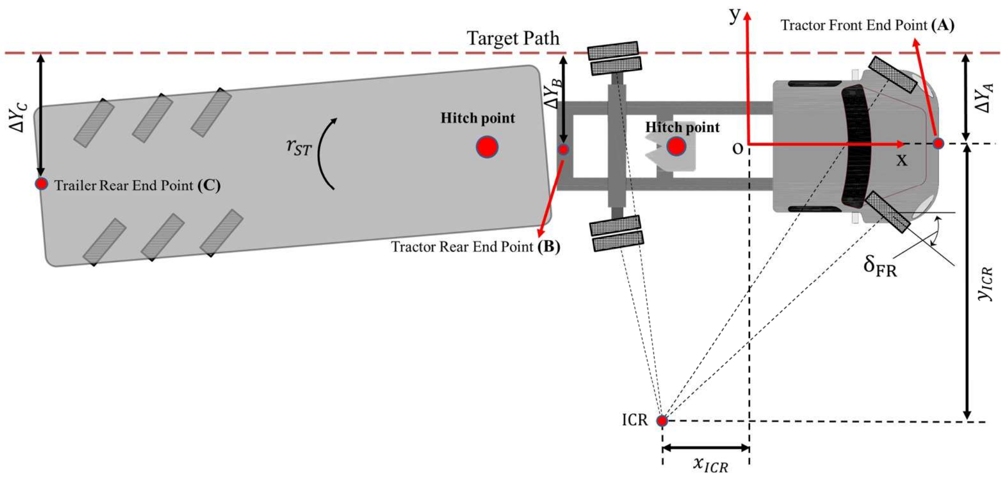

Figure 1. Parameter definition for the vehicle
200x97mm (300 x 300 DPI)

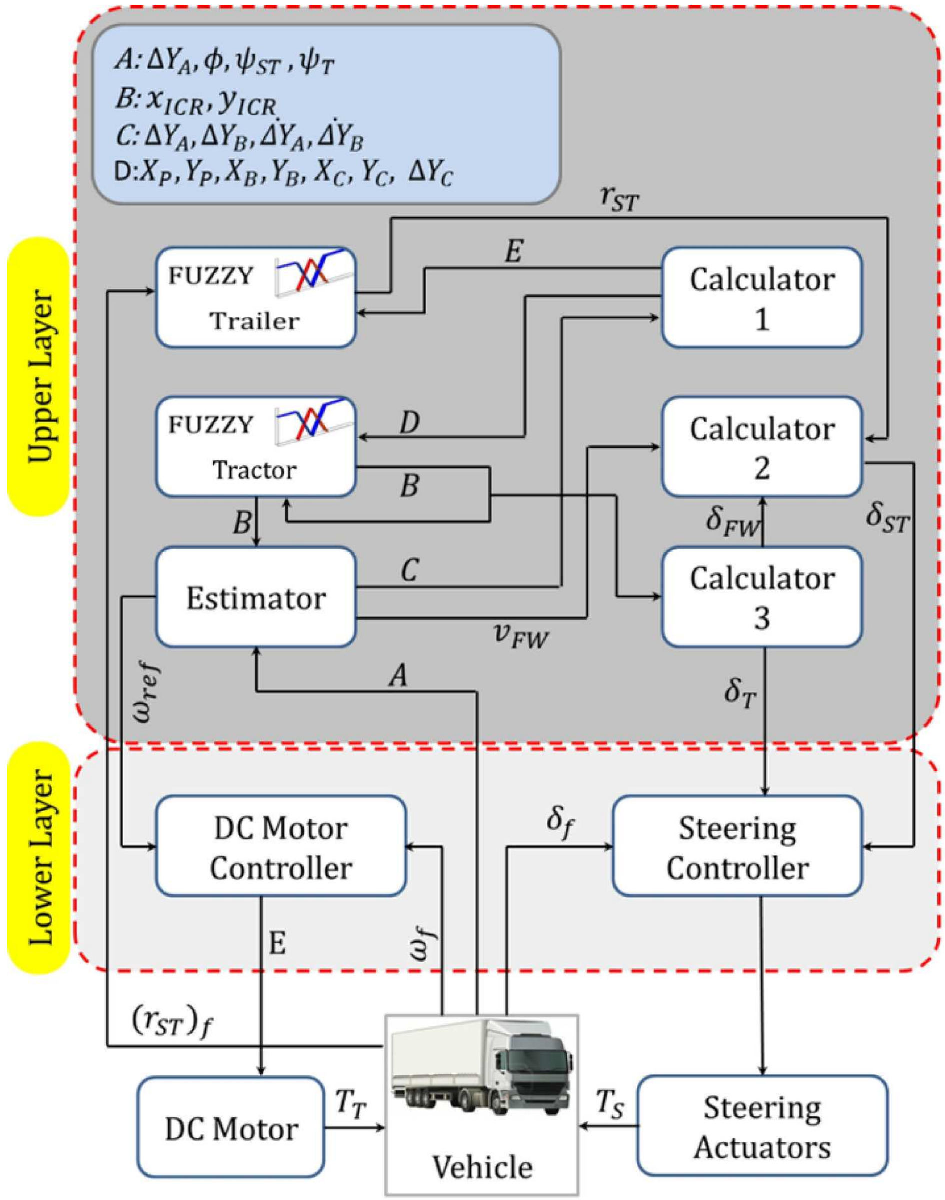

Figure 2. Block diagram of the proposed controller
212x271mm (300 x 300 DPI)

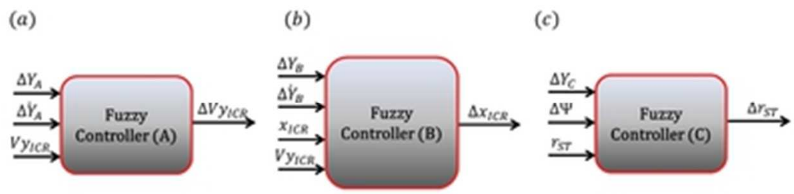

Figure 3. Fuzzy logic controllers
34x8mm (300 x 300 DPI)

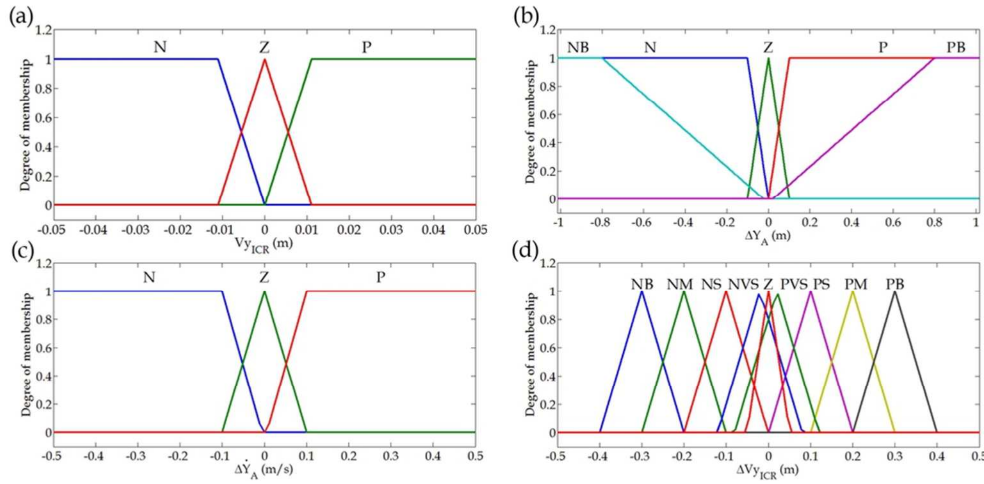

Figure 4. Membership functions for the controller (A)
88x42mm (300 x 300 DPI)

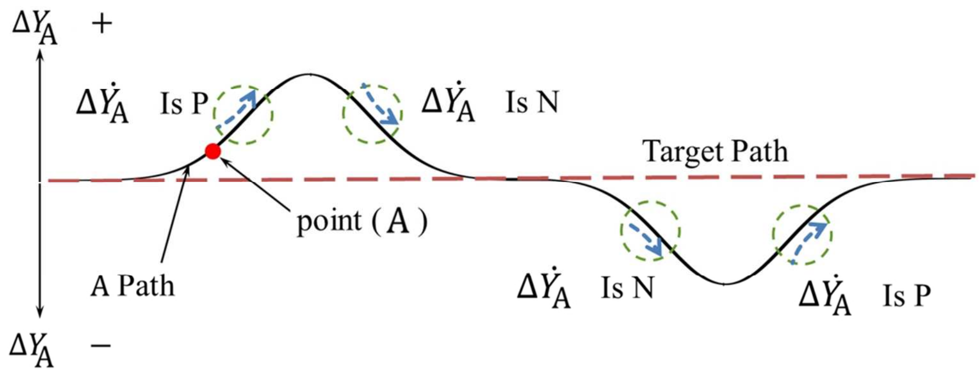

Figure 5. Relationship between a deviation and its derivative according to the target path
97x36mm (300 x 300 DPI)

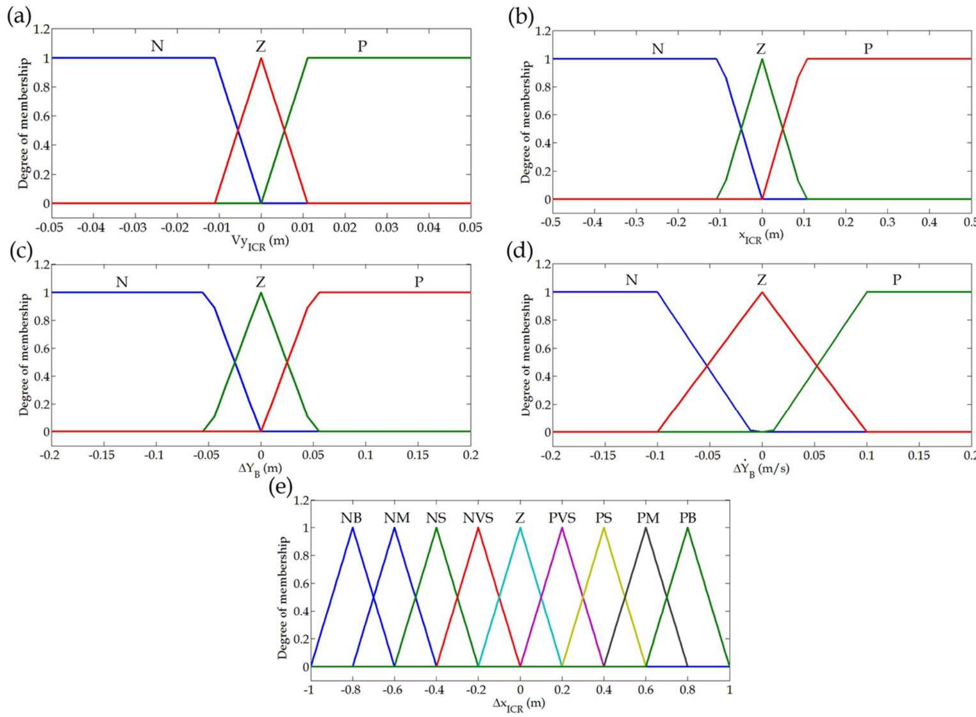

Figure 6. Membership functions for the controller (B)
133x94mm (300 x 300 DPI)

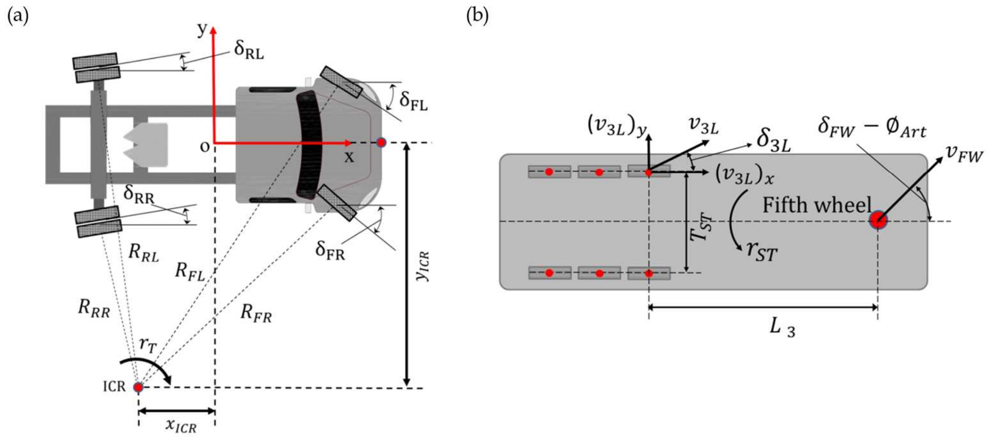

Figure 7. Steering angle calculation
217x95mm (300 x 300 DPI)

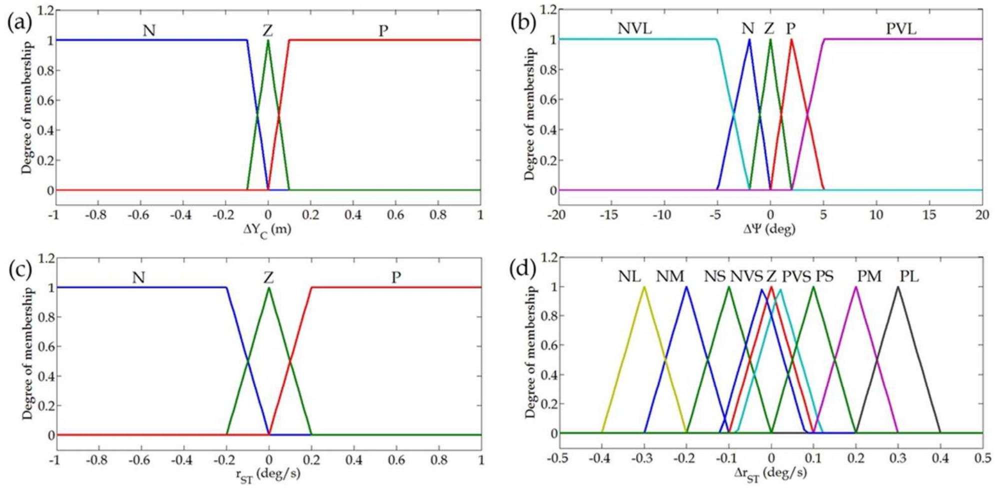

Figure 8. Membership functions for the controller (C)
91x45mm (300 x 300 DPI)

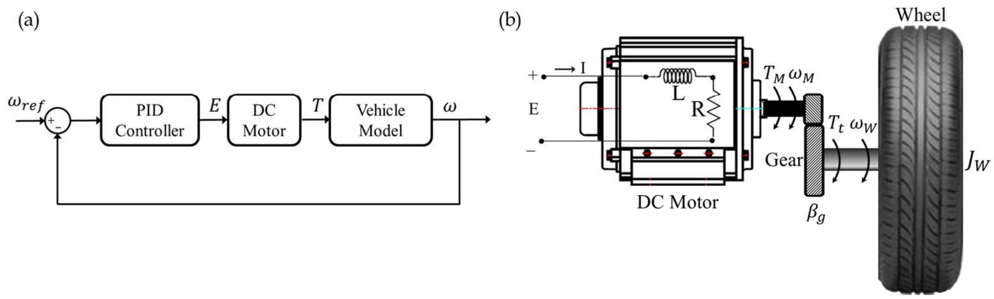

Figure 9. (a) Lower layer controller (b) scheme of torque transmission
149x44mm (300 x 300 DPI)

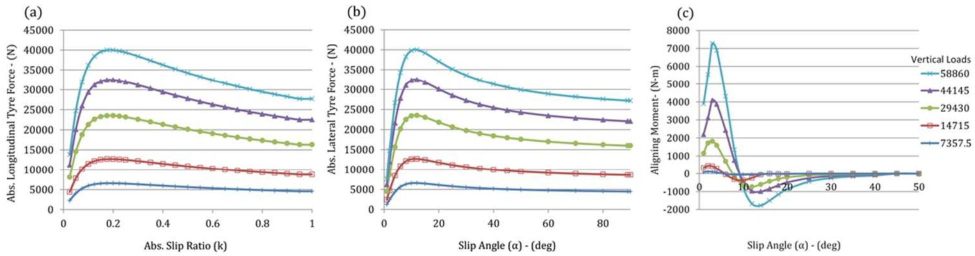

Figure 10. Shear forces and moments measured in tests - (a) Longitudinal force (b) Lateral force (c) Aligning moment
101x26mm (300 x 300 DPI)

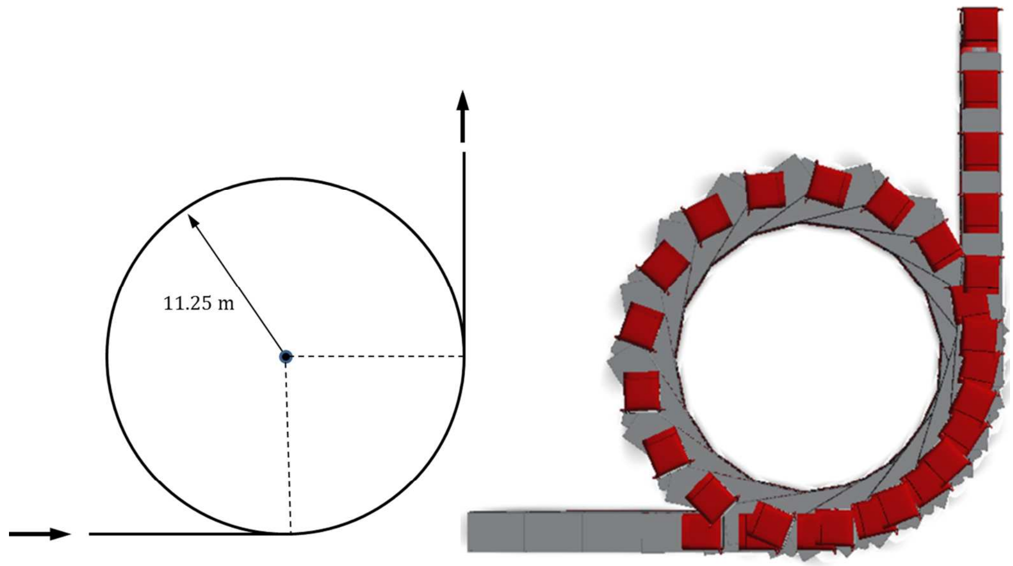

Figure 11. Roundabout maneuver path
206x120mm (300 x 300 DPI)

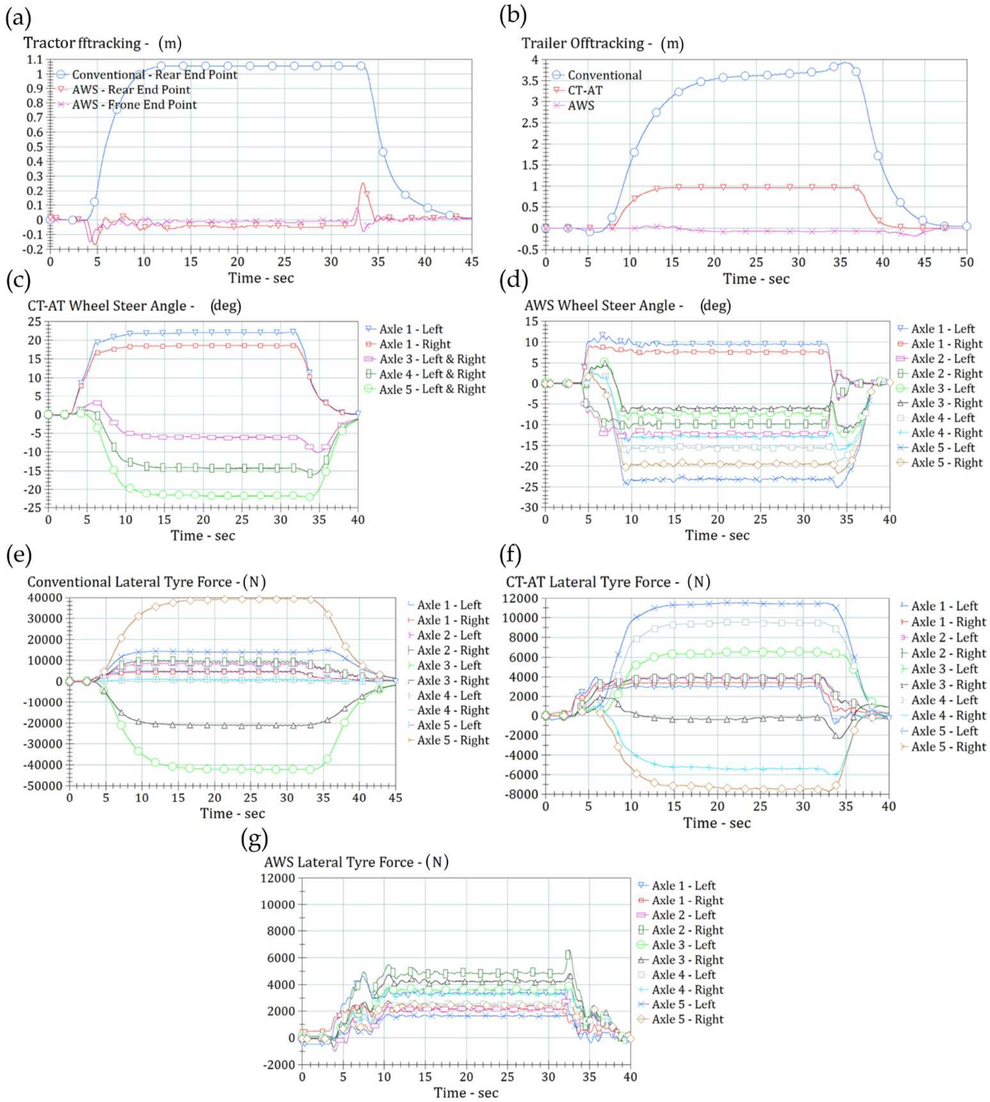

Figure 12. Simulation results of the roundabout maneuver
390x433mm (300 x 300 DPI)

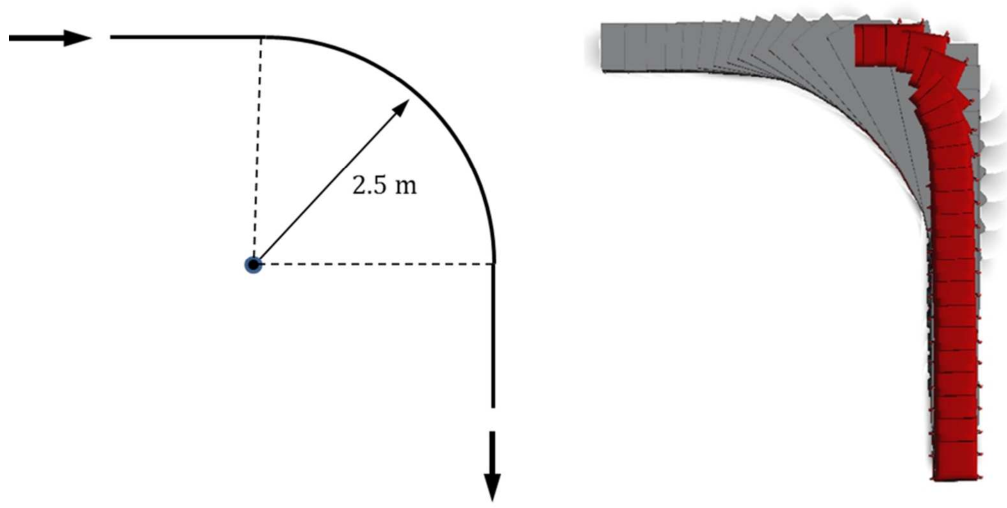

Figure 13. 90 degrees maneuver path
96x52mm (300 x 300 DPI)

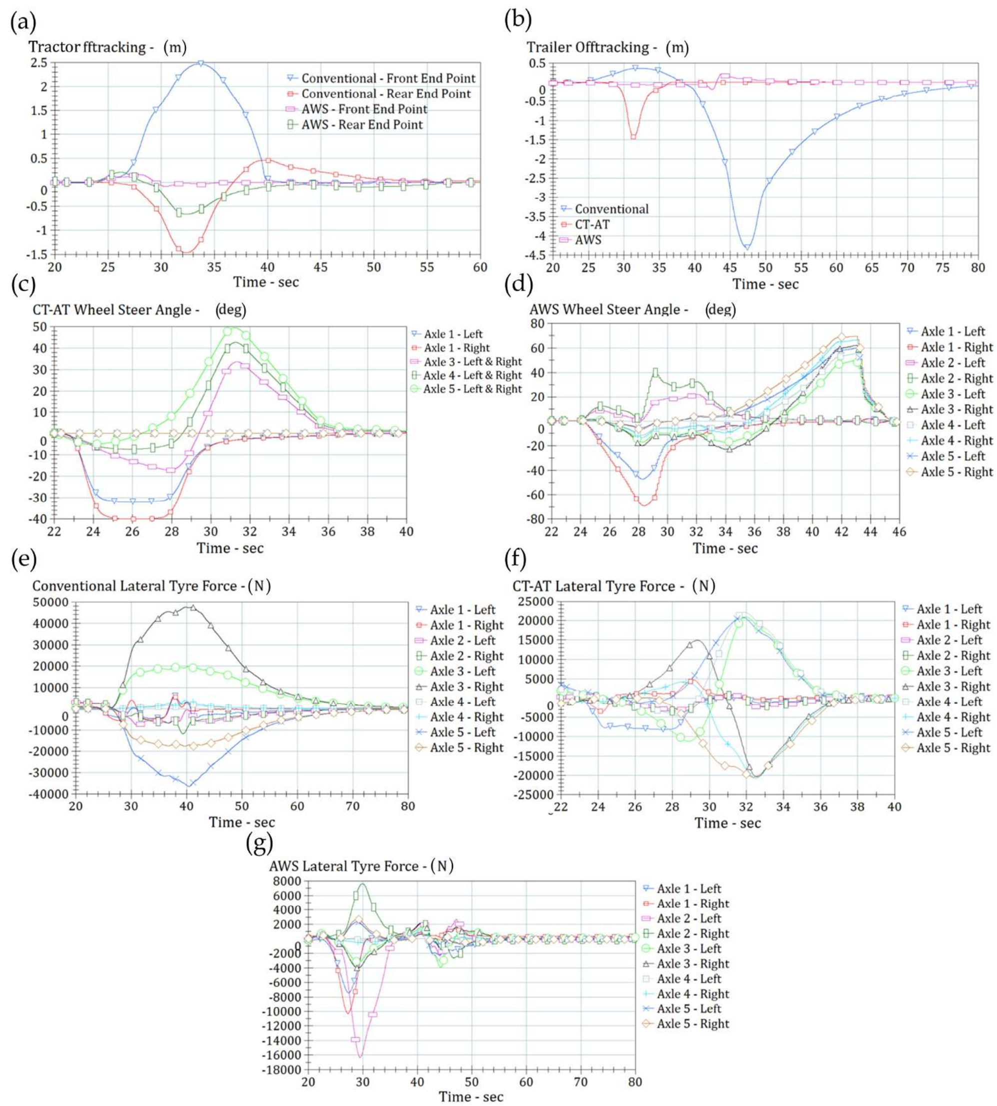

Figure 14. Simulation results of the 90 degrees maneuver
390x433mm (300 x 300 DPI)

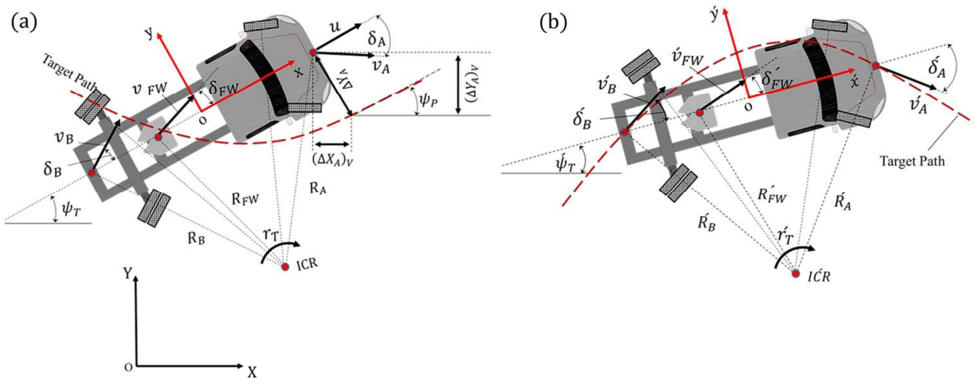

Figure 15. Parameter definition of (a) tractor and (b) tractor estimator
175x68mm (300 x 300 DPI)

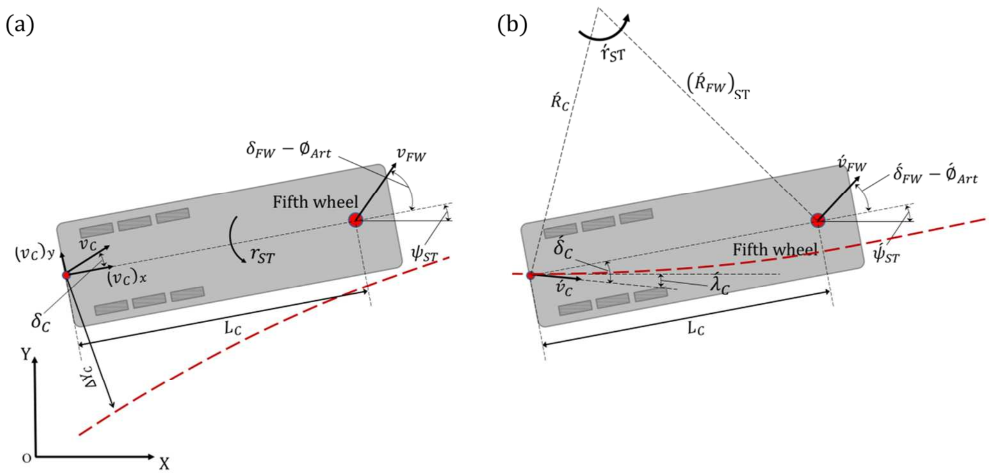

Figure 16. Parameter definition of (a) trailer and (b) trailer estimator
192x90mm (300 x 300 DPI)